Geophysical Research Letters

RESEARCH LETTER
10.1029/2024GL109927

Distinct Propagation to Agricultural Drought Between Two Severe Meteorological Droughts in the Korean Peninsula

Yoo-Geun Ham[1], **Yerim Jeong**[2], **and Eunkyo Seo**[3,4]

[1]Department of Environmental Planning, Graduate School of Environmental Studies, Seoul National University, Seoul, South Korea, [2]Environmental Planning Institute, Seoul National University, Seoul, South Korea, [3]Department of Environmental Atmospheric Sciences, Pukyong National University, Busan, South Korea, [4]Center for Ocean-Land-Atmosphere Studies, George Mason University, Fairfax, VA, USA

Key Points:

- Despite similar degrees of total precipitation deficits, soil moisture (SM) deficit was twice for 94–96 drought compared to 13–17 drought
- In 94–96 drought, precipitation deficit was robust during early phase, leading greater SM sensitivity to the precipitation shortages
- In 94-96 drought, the precipitation deficit occurred during dry seasons intensified the overall SM responses

Supporting Information:

Supporting Information may be found in the online version of this article.

Correspondence to:

Y.-G. Ham,
yoogeun@snu.ac.kr

Citation:

Ham, Y.-G., Jeong, Y., & Seo, E. (2024). Distinct propagation to agricultural drought between two severe meteorological droughts in the Korean Peninsula. *Geophysical Research Letters*, *51*, e2024GL109927. https://doi.org/10.1029/2024GL109927

Received 3 MAY 2024
Accepted 6 SEP 2024

Author Contributions:

Conceptualization: Yoo-Geun Ham
Formal analysis: Yerim Jeong
Funding acquisition: Yoo-Geun Ham
Investigation: Yerim Jeong
Methodology: Yoo-Geun Ham
Supervision: Yoo-Geun Ham
Visualization: Yerim Jeong
Writing – original draft: Yoo-Geun Ham
Writing – review & editing: Yoo-Geun Ham, Eunkyo Seo

Abstract Distinct responses in the soil moisture (SM) between the two most severe meteorological droughts in Korea are examined. Although total accumulated precipitation deficit during 1994–1996 drought was slightly less than in the 2013–2017 drought, 1994–1996 drought showed a record-breaking negative SM anomalies, while the accumulated negative SM anomalies during 2013–2017 were less than half of those in 1994–1996. In 1994–1996 case, robust precipitation deficits occurred early in the event, leading to subsequent precipitation shortages under dry conditions. In addition, precipitation deficit was observed not only during wet seasons but also throughout dry seasons. This amplifies the SM response, as the runoff volume remains relatively constant despite reduced precipitation in arid soil conditions, which eventually reduces soil water retention led by the precipitation deficit. Conversely, in 2013–2017 case, precipitation deficit occurred during later period of the event and wet seasons, which leads a moderate SM drying signals.

Plain Language Summary Understanding the process of how meteorological drought transitions into agricultural drought is essential for improving early warning systems and enhancing water resource management and mitigation strategies of drought on water availability and ecosystems. In South Korea, there are two most severe multi-year meteorological droughts in 1994–1996 and 2013–2017, however, its transition to the agricultural drought is quite different. It is found that the detailed timing of the precipitation deficit is crucial to understand the differences in the agricultural drought signal between two meteorological drought events. In 1994–1996 drought, precipitation deficits occurred early phase of the event, and were observed not only during wet seasons but also throughout dry seasons. This amplifies the overall soil moisture response. Conversely, in 2013–2017 case, precipitation deficit occurred during later period of the event and wet seasons, resulting in moderate agricultural drought signals.

1. Introduction

Soil moisture (SM) plays a crucial role in the hydrological cycle, exerting substantial influence over the exchange of heat between the Earth's land surface and the atmosphere, as well as critical biological processes (McColl et al., 2017; Seneviratne et al., 2010). Abrupt changes in SM provide an early warning for floods and droughts, and long-term SM variations are the key in estimating and predicting agricultural yields (Entekhabi et al., 2010).

Droughts can be generally classified into meteorological, agricultural, hydrological, and socioeconomic droughts (Wilhite & Glantz, 1985). Drought signals are initiated by the meteorological drought caused by the precipitation deficits, then, propagates to other types of droughts. Various climate factors is known to cause the meteorological drought in Korea (J. Y. Kim et al., 2017). The cyclonic circulations over the western north Pacific tend to induce warm season droughts by suppressing moist water transport from the south of the Korean Peninsula (M. Kwon, 2013; Myoung et al., 2020; K. H. Seo et al., 2011), whose intensity can be controlled by SST forcings over the north Pacific (K. H. Seo et al., 2011), subtropical Pacific (Ham et al., 2022), Indian Ocean (Ham et al., 2021; Xie et al., 2009), and tropical Atlantic (Ham et al., 2017). Additionally, the North Atlantic Oscillation (Ding & Wang, 2005; Sun et al., 2008; Sung et al., 2006; Z. Wu et al., 2009), or subpolar jets (Lau & Weng, 2002; Lau et al., 2000, 2004) has been recognized by altering Korean rainfall patterns.

In general, meteorological drought, often measured by Standardized Precipitation Index (SPI), and the other type of droughts exhibit a positive correlation with a time lag (Eltahir, 1998; Findell & Eltahir, 1997; Lee et al., 2022; Zheng & Eltahir, 1998). However, it is important to acknowledge the intricacies of the propagation mechanism of

the meteorological drought to other types of droughts due to the inherent nonlinearity of the system (Boé, 2013; Cook et al., 2006; Ford, Quiring, et al., 2015; Ford, Rapp, et al., 2015). For example, according to the Curve Number method developed by Soil Conservation Service (Mishra et al., 2003), SM response to the precipitation change is nonlinear due to the initial abstraction for the soil type with an infiltration (Bos et al., 2008). In more detail, background states (i.e., climate regimes and land cover) also can control the degree and speed of the propagation of the meteorological drought signal to the SM (E. Seo & Dirmeyer, 2022). Based on the water balance equation, a strong correlation between SM and precipitation is observed in drier and less vegetated climates associated with suppressed evapotranspiration (Sehler et al., 2019), referred to as water-limited regimes. The areas are sensitive to the land conditions and thus exerting feedback from land to atmosphere, in which the partitioning between sensible and latent fluxes is tied by the variability of the SM (E. Seo et al., 2024). Similarly, under the dry SM condition, the seasonal variations of SM and the propagation of SM anomalies from the surface to deeper layers are stronger than in normal years (W. Wu et al., 2002). This is associated with the fact that the retained fraction of the incoming precipitation tends to be low in regions with high annual mean surface SM, as both drainage and runoff tend to be high in these regions (McColl et al., 2017; W. Wu et al., 2002). In contrast, for large negative SM anomalies, the SM deficit from relatively modest negative precipitation anomalies can be substantially amplified by high evaporation (Seneviratne et al., 2006). It is further investigated that the soil properties such as texture, bulk density, and organic matter content play a role in understanding SM dynamics (Martínez-Fernández et al., 2021).

While the previously mentioned nonlinear propagation mechanism from meteorological drought to agricultural drought is generally assessed by analyzing droughts over relatively short time scales (M. Kwon et al., 2019; Lee et al., 2022; Shin et al., 2020; Zhao et al., 2016), however, that during the multi-year droughts have been rarely examined. This might be due to the lack of a number of multi-year meteorological drought events to fairly compare the differences in the agricultural drought signals. Fortunately, there were two severe multi-year meteorological droughts in Korean Peninsula, whose amplitude of the agricultural drought signal, measured by SM anomalies, were dramatically different. This provides an opportunity to reveal the physical mechanism of different propagation of the multi-year meteorological droughts to agricultural droughts.

The data and the land model used in this study are introduced in Section 2. Section 3 presents observational differences in SM responses between two multi-year meteorological drought events on the Korean Peninsula and their possible mechanisms. Section 4 presents idealized single-column land model experiment results and Section 5 provides a summary of key findings and discusses their implications.

2. Data and Methods

2.1. Data

The monthly evapotranspiration and column-integrated SM anomalies were obtained from the European Centre for Medium-Range Weather Forecasts (ECMWF) ERA5 reanalysis (Hersbach et al., 2023). This reanalysis data has a 0.25° × 0.25° covering the 1979–2021 period (42 years). The SM data encompass four layers with soil depths of 0–289 cm. We also utilized monthly precipitation data from 47 stations provided by the Korea Meteorological Administration (KMA) weather data service (Ham et al., 2022), which provide comprehensive coverage of South Korea.

We focused on the South-Korea-averaged drought indices as the drought signals in Korean Peninsula during both 94–96 and 13–17 cases were shown over the entire Korean Peninsula, and exhibited fewer regional differences (Ham et al., 2022; S. Kim et al., 2011). All variables derived by ERA5 is area-averaged over South Korea (i.e., 135°E–140°E, 34°N–38°N). To diagnose meteorological drought, we used the SPI derived by 47 station data (Guttman, 1998; McKee et al., 1993), which is known to easily facilitates quantitative analyses and has been widely applied across a range of fields (Dutta et al., 2015; Min et al., 2003; Tsakiris & Vangelis, 2004). In this study, the SPI12 was used by using 12-month averaged precipitation from January to December to diagnose long-lived drought conditions for each year.

2.2. Joint UK Land Environment Simulator (JULES)

The Joint UK Land Environment Simulator (JULES) is a widely used community land surface model, which serves as a land surface scheme in the Hadley Centre GCM (Best et al., 2011; Clark et al., 2011; Senior

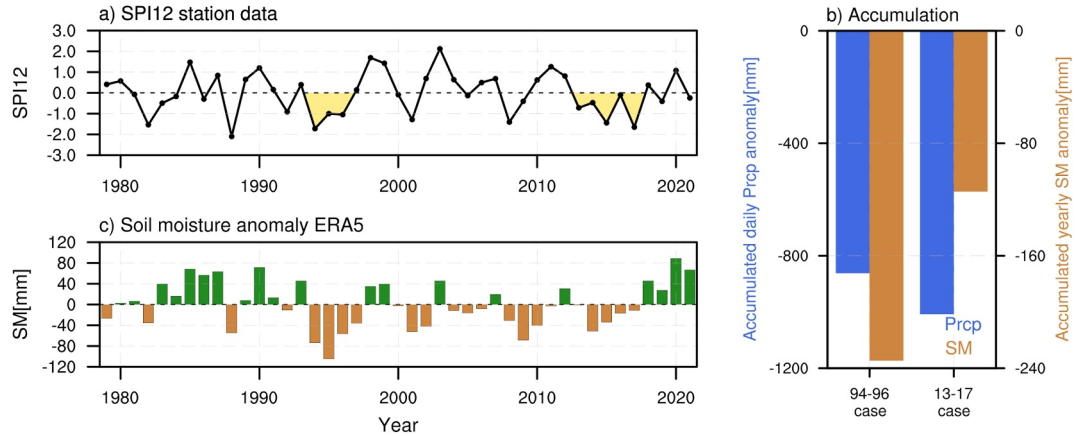

Figure 1. (a) Standardized Precipitation Index-12 during 1979–2021 obtained from the data derived from 47 stations in South Korea. (b) Accumulated daily-mean precipitation anomalies (unit: mm, blue bars), and the accumulated yearly-mean soil moisture (SM) anomalies (unit: mm, brown bars) in 1994–1996 and 2013–2017 meteorological drought cases over south Korea (135°E–140°E, 34°N–38°N). (c) Annual-mean SM anomalies (0–289 cm) (unit: mm) during 1979–2021 obtained via ERA5 reanalysis.

et al., 2020). It describes the physical, biophysical, and biochemical processes between the land surface and the atmosphere, and the multi-layer subsurface heat and water flux exchange processes (Cox et al., 1999). JULES employs the soil hydraulic model proposed by Brooks and Corey (1964) to characterize the soil water retention curve. And JULES models contain five vegetation (broadleaf, needleleaf trees, C_3, C_4 grass, shrubs) types and four non-vegetation (urban, lake, soil, ice) types. The parameters for each vegetation type are fixed in this study, by following the values in Clark et al. (2011).

In this study, we employed a single-column framework using JULES version 3.4.1 to perform simulations for the Korean Peninsula, as, both severe meteorological drought signals were exhibited fewer regional differences. The simulated results exhibit a single grid point with four vertical layers (0.1, 0.35, 1, and 3 m). It utilizes ERA5 data for meteorological forcings (i.e., 2 m specific humidity, 10 m wind speed, 2 m temperature, downward shortwave and longwave radiation at the surface, rainfall, and surface pressure) averaged over 125°E–130°E, 34°N–38°N every 30 min time step.

3. Distinct Soil Moisture Responses Between Two Major Multiyear Drought Events

Figure 1 shows the SPI12 and annual mean SM anomalies averaged from the data from January to December over the Korean Peninsula during 1979–2021. Instances with consecutive negative SPI12 for more than two years were observed in 1981–1984, 1994–1996, 2000–2001, 2008–2009, and 2013–2017, representing the multiyear meteorological drought events over the Korean Peninsula (J. S. Kim et al., 2017; Min et al., 2003). Note that these events are well matched to the drought events defined by using other meteorological drought indices (Bae et al., 2019; D. W. Kim et al., 2009). Among the multiyear drought events, two major meteorological drought events were identified during 1994–1996 (hereinafter referred to as Case 94–96) and 2013–2017 (hereinafter referred to as Case 13–17) in terms of total accumulated negative SPI12 during the entirety of the event periods (denoted by yellow areas in Figure 1a) (Ham et al., 2022; H. H. Kwon et al., 2016).

Despite the greater precipitation deficit in the 13–17 case (total accumulated daily precipitation anomalies from 1 January 2013 to 31 December 2017, amounting to −1,007.72 mm) compared to the 94–96 case (total accumulated daily precipitation anomalies from 1 January 1994 to 31 December 1996, totaling −861.77 mm) (blue lines in Figure 1b), the SM deficit derived by ERA5 data averaged over south Korea (135°E–140°E, 34°N–38°N) was much more excessive for the 94–96 case. The accumulated annual-mean SM anomaly from January 1994 to December 1996 is −234.54 mm, whereas that from January 2013 to December 2017 is only −114.33 mm. Therefore, the SM sensitivity to the precipitation deficit, defined as the ratio of the accumulated annual-mean SM anomalies to the accumulated precipitation anomalies during the whole period, is 0.27 for the 94–96 case and only 0.11 for the 13–17 case. This distinctive SM response to the precipitation deficit is evident in the time series of annual-mean SM anomalies from 1979 to 2021 (Figure 1c).

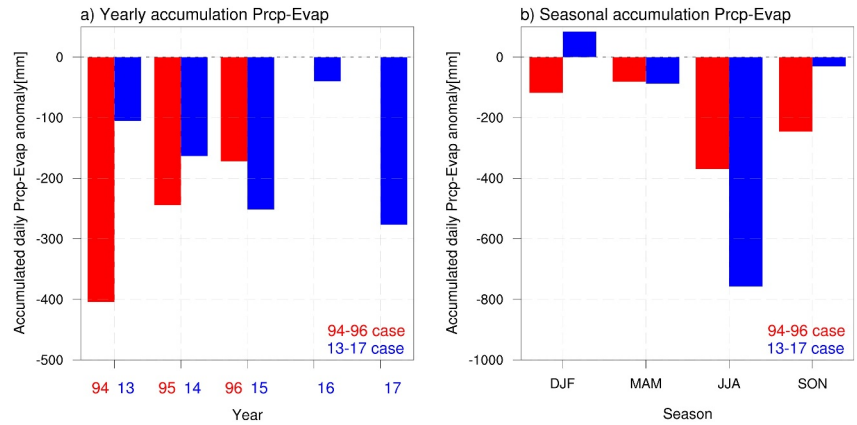

Figure 2. (a) Yearly and (b) seasonally accumulated precipitation minus evapotranspiration ($P - E$) for the 1994–1996 and 2013–2017 cases obtained via ERA5 reanalysis averaged over south Korea (135°E–140°E, 34°N–38°N). The $P - E$ values at the 4th (1997) and 5th year (1998) of the 94–96 case are not shown, as the meteorological drought event in the 94–96 case ceased in 1996.

To elucidate the mechanism underlying the distinct differences in SM responses between the two major meteorological drought events, Figure 2 displays yearly and seasonally accumulated daily $P - E$ anomalies for 94–96 and 13–17 cases. For the 94–96 case, negative $P - E$ anomalies are prominent in the earliest year (i.e., 1994), with their amplitude decreasing over time. In contrast, negative accumulated $P - E$ anomalies are relatively weak in the earliest year (i.e., 2013) and then strengthen during the following years (e.g., 2015 and 2017) for 13–17 case.

The systematic temporal difference in $P - E$ anomalies between the 94–96 case and the 13–17 case was also evident in the seasonally accumulated values during the entire drought period (i.e., 3 years for 94–96 case, and 5 years for 13–17 case) (Figure 2b) to compare with values in Figure 1 (i.e., total SM and precipitation deficits). For the 94–96 case, the precipitation deficit was evident for all seasons; negative accumulated $P - E$ anomalies were observed during boreal fall or winter seasons (September-October-November (SON) and December-January-February (DJF)), as well as the boreal summer season (June-July-August (JJA)). On the other hand, for the 13–17 case, excessive negative accumulated $P - E$ anomalies were observed during the JJA season, whereas those during other seasons were not clear. The accumulated $P - E$ anomalies even exhibited a positive value for the DJF season of the 94–96 case. Consequently, the precipitation deficit measured by the accumulated $P - E$ was relatively well distributed for all seasons and was also evident during dry seasons for the 94–96 case, whereas it was prominent during the wet season for the 13–17 case.

The detailed timing of the precipitation deficit can influence the overall sensitivity of SM to the total precipitation deficit. To illustrate this, we initially quantified SM sensitivity by calculating the ratio of SM anomalies averaged from 1 December to the subsequent 30 November to the accumulated precipitation deficit during the same period. Note that the general conclusion remains similar with a slightly different selection of the months for calculating an annual-mean value. To focus on the periods exhibiting drought conditions, the calculated SM sensitivity is presented only for years when precipitation from 1 December to the subsequent 30 November is negative.

Figure 3a shows a scatter plot between the initial SM anomalies, defined as the DJF SM anomalies, and the SM sensitivity during 1979–2021. As illustrated in the figure, SM sensitivity tends to be higher for years with initially drier SM anomalies. Based on Student's *t*-test, the correlation coefficient between the initial SM anomalies and SM sensitivity is −0.82 with a 99% confidence level. This implies that SM responses tend to be greater for initially drier conditions.

These findings suggest that the prominent precipitation deficit during the early phase of the 94–96 drought event contributes to enhance SM sensitivity by exhibiting subsequent precipitation deficits associated with the atmospheric teleconnections induced by the a large-scale land surface (Park & Schubert, 1997), or oceanic forcings (Yeo et al., 2019) under the dry condition. In the 94–96 case, the greatest precipitation deficit occurred in the first year, resulting in drier conditions during the early stages of the droughts. Under this arid SM condition in 1994, the negative SM anomalies to the precipitation deficit during the subsequent years (i.e., 1995 and 1996) can be

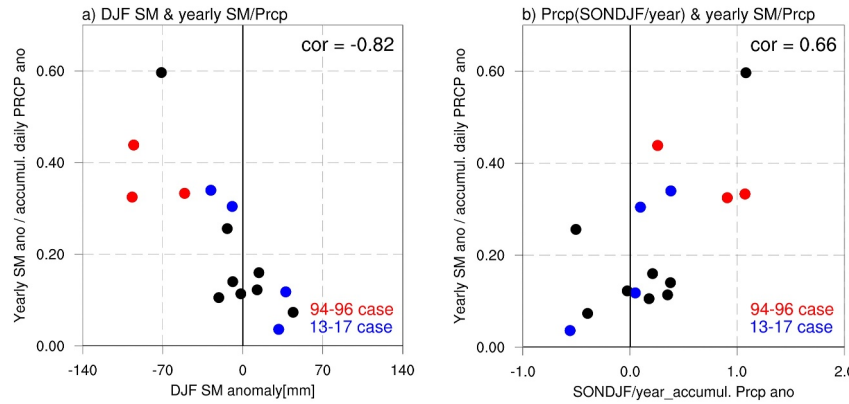

Figure 3. (a) Scatter diagram between the ratio of the yearly-averaged soil moisture (SM) anomaly to the yearly-accumulated precipitation anomaly and (a) DJF SM anomalies, and (b) the ratio of the precipitation deficit during the boreal fall (September-October-November) and winter (December-January-February) seasons to that during the whole year over south Korea. The values for the 94–96 and 13–17 cases are indicated in red and blue dots, respectively. Note that the yearly-averaged or -accumulated values were calculated by using the values from December to the subsequent November. The values are shown only for the years when the yearly-averaged precipitation anomaly was negative to focus on the drought conditions.

intensified. Consequently, overall negative SM anomalies can exhibit a record-breaking amplitude. On the other hand, in the 13–17 case, where the precipitation deficit is not prominent during the early stage (i.e., 2013 or 2014), the moderate SM condition weakens the overall SM sensitivity, and therefore 13–17 case fails to develop to the strong SM drought.

This nonlinear SM response to precipitation can be understood based on the following balance equation (Bos et al., 2008; Woodward et al., 2003):

$$Q = \frac{(P - I_a)^2}{P - I_a + S}, \tag{1}$$

where Q, P, I_a, S is an accumulated runoff depth, accumulated precipitation depth, initial abstraction, and maximum retention, respectively. Two retention variables (i.e., I_a, and S) can be merged into one variable by following the empirical relationship that $I_a = 0.2S$. Then, the equation can be modified as follows.

$$Q = \frac{(P - 0.2S)^2}{P + 0.8S}, \quad \text{for } P \geq 0.2S, \tag{2}$$

which exhibits a nonlinear relationship between P and Q for the soil type with a moderate infiltration S (Figure S2 in Supporting Information S1). Based on Equation 2, the runoff sensitivity to the precipitation (i.e., $\frac{\partial Q}{\partial P}$) can be derived as follows.

$$\frac{\partial Q}{\partial P} = 1 - \frac{S^2}{(P + 0.8S)^2} \tag{3}$$

According to the derivation, $\frac{\partial Q}{\partial P}$ is proportional to P: precipitation changes lead weaker runoff changes in a dry regime (i.e., less P). As a result, the change in the SM retention ΔF, which is simply proportional to $\Delta P - \Delta Q$, can be written as follows.

$$\Delta F \approx \Delta P - \Delta Q = \left(1 - \left[1 - \frac{S^2}{(P + 0.8S)^2}\right]\right)\Delta P = \frac{S^2}{(P + 0.8S)^2}\Delta P \tag{4}$$

This demonstrates that the amount of the SM deficit (i.e., negative ΔF) by precipitation deficit (i.e., negative ΔP) is greater in a dry regime (i.e., less P). On the other hand, once a shortage of precipitation is given during the wet season, the total amount of precipitation may not be severely insufficient; therefore, the soil drought signal can be less prominent.

Applying the same principle, SM sensitivity tends to be higher in years when the precipitation deficit is relatively larger during dry seasons (e.g., the boreal fall and winter seasons in Korea, as they are the off-monsoon seasons). Figure 3b presents a scatter diagram between SM sensitivity and the ratio of precipitation deficit during boreal SON and DJF seasons to that during the whole year (from December to the subsequent November). The correlation coefficient between them is 0.66 with a 99% confidence level based on Student's t-test, clearly demonstrating that SM sensitivity tends to be greater when the precipitation deficit is mostly within the dry seasons.

4. Idealized JULES Experiments

In this section, we utilized JULES to support our observational findings. First, to assess a capability of the JULES in SM, we performed a long-term JULES simulation from 1979 to 2021 by prescribing the daily meteorological forcings (Figure S1 in Supporting Information S1). Annual-mean SM anomalies over Korea in JULES simulation successfully mimics those in the SM reanalysis (Figure 1c); the temporal correlation coefficient of the annual-mean SM anomalies between the JULES simulation and the reanalysis from 1979 to 2021 is 0.83. More importantly, the systematic stronger SM deficits during 1994–1996 compared to that during 2013–2017 is also evident in the JULES simulations. This indicates that the JULES is suitable for examining the systematic difference in the differences in the SM responses between two strongest meteorological droughts in South Korea.

Next, we performed a series of the idealized JULES experiments to support our arguments. In the control experiment, spanning from 1979 to 2022, 1-year JULES simulations starting on 1 December (CTL_DJF) or 1 June (CTL_JJA) of each year were performed by prescribing daily precipitation at the corresponding time. For other atmospheric forcings, annual mean climatological values averaged from 1979 to 2022 were prescribed. Therefore, the year-to-year difference and the seasonal cycle in the results of the JULES experiments were solely due to the precipitation. In the EXP_DJF, we subtracted monthly precipitation amounts of 10 mm for December, 15 mm for January, and 10 mm for February from the precipitation input in CTL_DJF. For the EXP_JJA, the same amount of precipitation was subtracted during the JJA season (i.e., subtract 10 mm for June, 15 mm for July, and 10 mm for August) from the precipitation input in CTL_JJA. The precipitation input for the EXP for each day is obtained as follows.

$$P_i(\mathrm{EXP}) = \frac{\sum_{i=1}^{n} P_i(\mathrm{CTL}) - \alpha}{\sum_{i=1}^{n} P_i(\mathrm{CTL})} \times P_i(\mathrm{CTL}) \tag{5}$$

where n, α, P_i(CTL), and P_i(EXP) represent the total number of days in a month, a prescribed monthly accumulated precipitation deficit (e.g., 10 mm for June in EXP_JJA), the daily precipitation at the ith day of the month for the control experiment, and that for the EXP, respectively.

Differences in the simulation results between EXP_DJF and CTL_DJF, and EXP_JJA and CTL_JJA indicate whether the precipitation deficit occurred during boreal winter and summer seasons, respectively. The initial conditions are obtained through long-term JULES simulations on the corresponding calendar day (e.g., 1 June for JJA experiments, 1 December for DJF experiments) from 1979 to 2021 with realistic atmospheric forcings. The results for each year are considered as the ensemble members of each experiment, and therefore each experiment has 42 ensemble members.

Figure 4a presents a scatter diagram with 42 ensemble members between the SM averaged from the surface to 10 cm of CTL_DJF experiments at DJF and the SM sensitivity, defined by the difference (i.e., EXP_DJF minus CTL_DJF) in the SM averaged during 1 December to the subsequent 30 November divided by the difference in the precipitation averaged during the same period. It is important to note that, as the precipitation difference between EXP_DJF and CTL_DJF is identical for all ensemble members, SM sensitivity is solely dependent on the

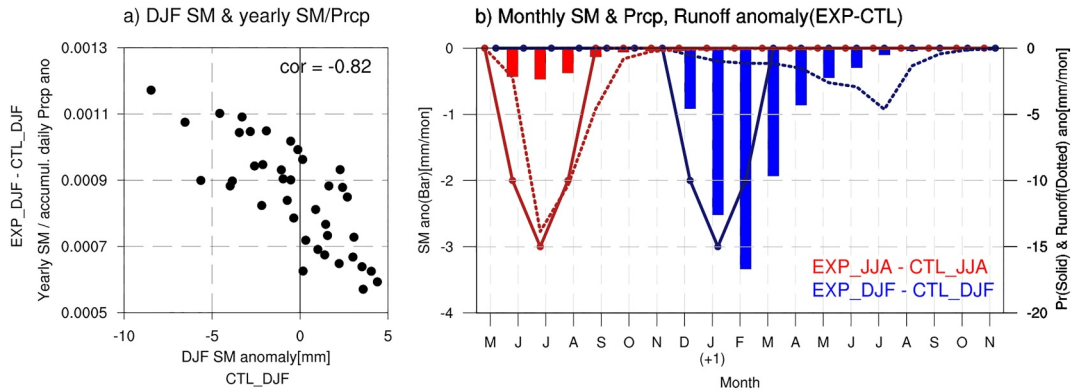

Figure 4. (a) Scatter diagram between the ratio of the yearly-averaged soil moisture (SM) difference to the yearly-accumulated precipitation difference (EXP_DJF minus CTL_DJF) and DJF SM anomalies (from surface to 10 cm depth) simulated in CTL_DJF. Note that the yearly-averaged or -accumulated values were calculated using the values from December to the subsequent November. (b) Simulated monthly time series of the surface-layer SM (bars), precipitation (solid line), and total runoff (dotted line) differences between the EXP_JJA and CTL_JJA (red) or the EXP_DJF and CTL_DJF (blue) experiments.

SM responses to the prescribed identical precipitation deficit. The simulated results strongly support the observational findings that the initially drier condition tends to increase SM sensitivity. The correlation coefficient between them is −0.82, which is over the 99% confidence level based on Student's *t*-test. This supports our arguments that the timing of the precipitation deficit according to the phase of the drought leads a dramatic difference in the overall propagation degree of the meteorological drought to SM drought.

In Figure 4b, we calculated an ensemble-averaged time-series of the SM and precipitation differences between EXP_JJA and CTL_JJA (red), and EXP_DJF and CTL_DJF (blue). For the precipitation deficit during JJA, the reduction of the runoff is also clearly shown much as the precipitation deficit. Due to this compensation between the precipitation and runoff deficits, as a result, the negative SM anomalies were relatively weak, with a value of approximately −0.5 mm from June to September. On the other hand, for the precipitation deficit during DJF, the runoff is not decreased much as the precipitation deficits, the soil drought signal was stronger and was sustained for a longer period. The negative SM difference for the prescribed precipitation deficit during the JFM season mostly varied between −2 and −4 mm and lasted from December to June of the next year. As a result, the time-averaged negative SM anomaly for the identical precipitation deficit in DJF experiments is almost six times (i.e., −0.81 mm) that for the JJA experiments (i.e., −0.13 mm). This demonstrates that, when the negative precipitation anomaly occurs during the season of climatological dryness (i.e., DJF season in this case), it leads to a stronger negative soil drought anomalies by the nonlinear relationship between the precipitation and the runoff. Due to a dramatic differences in the background states between the seasons in Korea, the timing of the precipitation deficit according to the season is a critical driver of the dramatic differences in the soil drought signal.

Note that the reduction in the evapotranspiration by given precipitation deficit is greater during DJF experiments, rather than the JJA experiments (Figure S3 in Supporting Information S1), which means that the evapotranspiration would not be responsible for the stronger SM drought signal in DJF experiments.

5. Summary and Discussion

In this study, the dramatic difference in the SM anomalies between two major meteorological drought events that occurred in Korea during 1994–1996 and 2013–2017 is explored. Despite a total precipitation deficit is greater in the 13–17 case, the SM deficit was almost twice as much during the 94–96 case. In the 94–96 case, the precipitation deficit was robust during the early stage of the event, occurring not only during the wet seasons (i.e., boreal summer season) but also during the dry seasons (i.e., boreal fall and winter seasons). In contrast, in 13–17 case, the precipitation deficit occurred during the late period of the event, predominantly during the boreal summer season.

The precipitation deficit during the early phase in the 94–96 case causes a following precipitation shortage in a drought-stricken condition, intensifying the SM responses. Conversely, in 13–17 case, the precipitation deficit is

modest during the early phase of the drought, then, the precipitation deficit associated with the atmospheric teleconnections induced by large-scale oceanic forcings is followed under modestly dry conditions. Therefore, the overall SM response is weakened due to a relatively higher drainage and runoff rate. Additionally, the intense precipitation scarcity during the dry seasons in the 94–96 case also contributes to increasing the SM response. This is distinct from the 13–17 case, where the precipitation deficit mostly occurs during the wet seasons, when the precipitation amount would not be severely insufficient due to higher climatological precipitation. Idealized JULES experiments support our main arguments.

The different characteristics between 1994–1996 and 2013–2017 droughts can be also understood as the those in two regimes of the land-atmosphere coupling; a water-limited, and energy-limited regimes (Pendergrass et al., 2020). Under the water-limited regime, SM controls the partitioning of surface heat fluxes and the near-surface atmospheric conditions. Since such land-atmosphere feedback typically operates under dry condition, 1994–1996 drought, which is particularly caused in the fall/winter precipitation deficit, would be the case. As the SM involves as a key variable for drought development in the water-limited regime, the negative SM responses to the precipitation deficit can be exaggerated during 1994–1996 drought. On the other hand, Potential ET (which depends on temperature, radiation, humidity, and wind) is known to serve as a driver under energy-limited regime, where atmospheric conditions (i.e., large-scale circulation) influence the land surface states (see Figure 2 in E. Seo et al. (2024)). The majority of energy-limited coupling is shown during transitional seasons, therefore, drought event in 2013–2017, which is primary caused in the summer precipitation deficit, would be the case.

Data Availability Statement

ERA5 meteorological data, provided by the European Centre for Medium-Range Weather Forecasts (ECMWF) (Hersbach et al., 2023). Korea Meteorological Administration (KMA) weather data service can be downloaded at https://data.kma.go.kr/data/grnd/selectAsosRltmList.do?pgmNo=36. To retrieve the necessary variables, first choose the data format as monthly. Then, select the desired period, stations, and variables. Finally, download the CSV files from the list that appears in the search outputs.

Acknowledgments
This work was supported by the New Faculty Startup Fund from Seoul National University. Y.-G. Ham was supported by the Korea Meteorological Administration Research and Development Program under Grant KMI2018-07010.

References

Bae, H., Ji, H., Lim, Y. J., Ryu, Y., Kim, M. H., & Kim, B. J. (2019). Characteristics of drought propagation in South Korea: Relationship between meteorological, agricultural, and hydrological droughts. *Natural Hazards*, *99*(1), 1–16. https://doi.org/10.1007/s11069-019-03676-3

Best, M. J., Pryor, M., Clark, D. B., Rooney, G. G., Essery, R., Ménard, C. B., et al. (2011). The joint UK land environment simulator (JULES), model description–Part 1: Energy and water fluxes. *Geoscientific Model Development*, *4*(3), 677–699. https://doi.org/10.5194/gmd-4-677-2011

Boé, J. (2013). Modulation of soil moisture–precipitation interactions over France by large scale circulation. *Climate Dynamics*, *40*(3), 875–892. https://doi.org/10.1007/s00382-012-1380-6

Bos, M. G., Kselik, R. A., Allen, R. G., & Molden, D. (2008). *Water requirements for irrigation and the environment*. Springer Science & Business Media.

Brooks, R. H., & Corey, A. T. (1964). *Hydraulic properties of porous media* (Vol. 3, p. 37). Colorado State University Hydrology Papers.

Clark, D. B., Mercado, L. M., Sitch, S., Jones, C. D., Gedney, N., Best, M. J., et al. (2011). The joint UK land environment simulator (JULES), model description–Part 2: Carbon fluxes and vegetation dynamics. *Geoscientific Model Development*, *4*(3), 701–722. https://doi.org/10.5194/gmd-4-701-2011

Cook, B. I., Bonan, G. B., & Levis, S. (2006). Soil moisture feedbacks to precipitation in southern Africa. *Journal of Climate*, *19*(17), 4198–4206. https://doi.org/10.1175/jcli3856.1

Cox, P. M., Betts, R. A., Bunton, C. B., Essery, R. L. H., Rowntree, P. R., & Smith, J. (1999). The impact of new land surface physics on the GCM simulation of climate and climate sensitivity. *Climate Dynamics*, *15*(3), 183–203. https://doi.org/10.1007/s003820050276

Ding, Q., & Wang, B. (2005). Circumglobal teleconnection in the Northern Hemisphere summer. *Journal of Climate*, *18*(17), 3483–3505. https://doi.org/10.1175/jcli3473.1

Dutta, D., Kundu, A., Patel, N. R., Saha, S. K., & Siddiqui, A. R. (2015). Assessment of agricultural drought in Rajasthan (India) using remote sensing derived vegetation condition index (VCI) and standardized precipitation index (SPI). *The Egyptian Journal of Remote Sensing and Space Science*, *18*(1), 53–63. https://doi.org/10.1016/j.ejrs.2015.03.006

Eltahir, E. A. (1998). A soil moisture–rainfall feedback mechanism: 1. Theory and observations. *Water Resources Research*, *34*(4), 765–776. https://doi.org/10.1029/97wr03499

Entekhabi, D., Njoku, E. G., O'neill, P. E., Kellogg, K. H., Crow, W. T., Edelstein, W. N., et al. (2010). The soil moisture active passive (SMAP) mission. *Proceedings of the IEEE*, *98*(5), 704–716. https://doi.org/10.1109/jproc.2010.2043918

Findell, K. L., & Eltahir, E. A. (1997). An analysis of the soil moisture-rainfall feedback, based on direct observations from Illinois. *Water Resources Research*, *33*(4), 725–735. https://doi.org/10.1029/96wr03756

Ford, T. W., Quiring, S. M., Frauenfeld, O. W., & Rapp, A. D. (2015). Synoptic conditions related to soil moisture-atmosphere interactions and unorganized convection in Oklahoma. *Journal of Geophysical Research: Atmospheres*, *120*(22), 11–519. https://doi.org/10.1002/2015jd023975

Ford, T. W., Rapp, A. D., Quiring, S. M., & Blake, J. (2015). Soil moisture–precipitation coupling: Observations from the Oklahoma Mesonet and underlying physical mechanisms. *Hydrology and Earth System Sciences*, *19*(8), 3617–3631. https://doi.org/10.5194/hess-19-3617-2015

Guttman, N. B. (1998). Comparing the Palmer drought index and the standardized precipitation index 1. *JAWRA Journal of the American Water Resources Association*, *34*(1), 113–121. https://doi.org/10.1111/j.1752-1688.1998.tb05964.x

Ham, Y. G., Chikamoto, Y., Kug, J. S., Kimoto, M., & Mochizuki, T. (2017). Tropical Atlantic-Korea teleconnection pattern during boreal summer season. *Climate Dynamics*, *49*(7–8), 2649–2664. https://doi.org/10.1007/s00382-016-3474-z

Ham, Y. G., Kang, S. Y., Jeong, Y., Jeong, J. H., & Li, T. (2022). Large-scale sea surface temperature forcing contributed to the 2013–17 record-breaking meteorological drought in the Korean Peninsula. *Journal of Climate*, *35*(12), 3767–3783. https://doi.org/10.1175/jcli-d-21-0545.1

Ham, Y. G., Kim, J. G., Lee, J. G., Li, T., Lee, M. I., Son, S. W., & Hyun, Y. K. (2021). The origin of systematic forecast errors of extreme 2020 East Asian Summer Monsoon rainfall in GloSea5. *Geophysical Research Letters*, *48*(16), e2021GL094179. https://doi.org/10.1029/2021gl094179

Hersbach, H., Bell, B., Berrisford, P., Biavati, G., Horányi, A., Muñoz Sabater, J., et al. (2023). ERA5 monthly averaged data on single levels from 1940 to present [Dataset]. *Copernicus Climate Change Service (C3S) Climate Data Store (CDS)*. https://doi.org/10.24381/cds.f17050d7

Kim, D. W., Byun, H. R., & Choi, K. S. (2009). Evaluation, modification, and application of the effective drought index to 200-year drought climatology of Seoul, Korea. *Journal of Hydrology*, *378*(1–2), 1–12. https://doi.org/10.1016/j.jhydrol.2009.08.021

Kim, J. S., Seo, G. S., Jang, H. W., & Lee, J. H. (2017). Correlation analysis between Korean spring drought and large-scale teleconnection patterns for drought forecasting. *KSCE Journal of Civil Engineering*, *21*(1), 458–466. https://doi.org/10.1007/s12205-016-0580-8

Kim, J. Y., Seo, K. H., Son, J. H., & Ha, K. J. (2017). Development of statistical prediction models for Changma precipitation: An ensemble approach. *Asia-Pacific Journal of Atmospheric Sciences*, *53*(2), 207–216. https://doi.org/10.1007/s13143-017-0027-2

Kim, S., Kim, B., Ahn, T. J., & Kim, H. S. (2011). Spatio-temporal characterization of Korean drought using severity–area–duration curve analysis. *Water and Environment Journal*, *25*(1), 22–30. https://doi.org/10.1111/j.1747-6593.2009.00184.x

Kwon, H. H., Lall, U., & Kim, S. J. (2016). The unusual 2013–2015 drought in South Korea in the context of a multicentury precipitation record: Inferences from a nonstationary, multivariate, Bayesian copula model. *Geophysical Research Letters*, *43*(16), 8534–8544. https://doi.org/10.1002/2016gl070270

Kwon, M. (2013). Diagnosis of Northeast Asian summer precipitation using the western North Pacific subtropical high index. *Journal of the Korean Earth Science Society*, *34*(1), 102–106. https://doi.org/10.5467/jkess.2013.34.1.102

Kwon, M., Kwon, H. H., & Han, D. (2019). Spatio-temporal drought patterns of multiple drought indices based on precipitation and soil moisture: A case study in South Korea. *International Journal of Climatology*, *39*(12), 4669–4687. https://doi.org/10.1002/joc.6094

Lau, K. M., Kim, K. M., & Yang, S. (2000). Dynamical and boundary forcing characteristics of regional components of the Asian summer monsoon. *Journal of Climate*, *13*(14), 2461–2482. https://doi.org/10.1175/1520-0442(2000)013<2461:dabfco>2.0.co;2

Lau, K. M., Lee, J. Y., Kim, K. M., & Kang, I. S. (2004). The North Pacific as a regulator of summertime climate over Eurasia and North America. *Journal of Climate*, *17*(4), 819–833. https://doi.org/10.1175/1520-0442(2004)017<0819:tnpaar>2.0.co;2

Lau, K. M., & Weng, H. (2002). Recurrent teleconnection patterns linking summertime precipitation variability over East Asia and North America. *Journal of the Meteorological Society of Japan. Ser. II*, *80*(6), 1309–1324. https://doi.org/10.2151/jmsj.80.1309

Lee, J., Kim, Y., & Wang, D. (2022). Assessing the characteristics of recent drought events in South Korea using WRF-hydro. *Journal of Hydrology*, *607*, 127459. https://doi.org/10.1016/j.jhydrol.2022.127459

Martínez-Fernández, J., González-Zamora, A., & Almendra-Martín, L. (2021). Soil moisture memory and soil properties: An analysis with the stored precipitation fraction. *Journal of Hydrology*, *593*, 125622. https://doi.org/10.1016/j.jhydrol.2020.125622

McColl, K. A., Alemohammad, S. H., Akbar, R., Konings, A. G., Yueh, S., & Entekhabi, D. (2017). The global distribution and dynamics of surface soil moisture. *Nature Geoscience*, *10*(2), 100–104. https://doi.org/10.1038/ngeo2868

McKee, T. B., Doesken, N. J., & Kleist, J. (1993). The relationship of drought frequency and duration to time scales. In *Proceedings of the 8th conference on applied climatology* (Vol. 17, No. (22), pp. 179–183).

Min, S. K., Kwon, W. T., Park, E. H., & Choi, Y. (2003). Spatial and temporal comparisons of droughts over Korea with East Asia. *International Journal of Climatology: A Journal of the Royal Meteorological Society*, *23*(2), 223–233. https://doi.org/10.1002/joc.872

Mishra, S. K., Singh, V. P., Mishra, S. K., & Singh, V. P. (2003). SCS-CN method. In *Soil conservation service curve number (SCS-CN) methodology* (pp. 84–146).

Myoung, B., Rhee, J., & Yoo, C. (2020). Long-lead predictions of warm season droughts in South Korea using North Atlantic SST. *Journal of Climate*, *33*(11), 4659–4677. https://doi.org/10.1175/jcli-d-19-0082.1

Park, C. K., & Schubert, S. D. (1997). On the nature of the 1994 East Asian summer drought. *Journal of Climate*, *10*(5), 1056–1070. https://doi.org/10.1175/1520-0442(1997)010<1056:otnote>2.0.co;2

Pendergrass, A. G., Meehl, G. A., Pulwarty, R., Hobbins, M., Hoell, A., AghaKouchak, A., et al. (2020). Flash droughts present a new challenge for subseasonal-to-seasonal prediction. *Nature Climate Change*, *10*(3), 191–199. https://doi.org/10.1038/s41558-020-0709-0

Sehler, R., Li, J., Reager, J. T., & Ye, H. (2019). Investigating relationship between soil moisture and precipitation globally using remote sensing observations. *Journal of Contemporary Water Research & Education*, *168*(1), 106–118. https://doi.org/10.1111/j.1936-704x.2019.03324.x

Seneviratne, S. I., Corti, T., Davin, E. L., Hirschi, M., Jaeger, E. B., Lehner, I., et al. (2010). Investigating soil moisture–climate interactions in a changing climate: A review. *Earth-Science Reviews*, *99*(3–4), 125–161. https://doi.org/10.1016/j.earscirev.2010.02.004

Seneviratne, S. I., Koster, R. D., Guo, Z., Dirmeyer, P. A., Kowalczyk, E., Lawrence, D., et al. (2006). Soil moisture memory in AGCM simulations: Analysis of global land–atmosphere coupling experiment (GLACE) data. *Journal of Hydrometeorology*, *7*(5), 1090–1112. https://doi.org/10.1175/jhm533.1

Senior, C. A., Jones, C. G., Wood, R. A., Sellar, A., Belcher, S., Klein-Tank, A., et al. (2020). UK community Earth system modeling for CMIP6. *Journal of Advances in Modeling Earth Systems*, *12*(9), e2019MS002004. https://doi.org/10.1029/2019ms002004

Seo, E., & Dirmeyer, P. A. (2022). Improving the ESA CCI daily soil moisture time series with physically based land surface model datasets using a Fourier time-filtering method. *Journal of Hydrometeorology*, *23*(3), 473–489. https://doi.org/10.1175/jhm-d-21-0120.1

Seo, E., Dirmeyer, P. A., Barlage, M., Wei, H., & Ek, M. (2024). Evaluation of land–atmosphere coupling processes and climatological bias in the UFS global coupled model. *Journal of Hydrometeorology*, *25*(1), 161–175. https://doi.org/10.1175/jhm-d-23-0097.1

Seo, K. H., Son, J. H., & Lee, J. Y. (2011). A new look at Changma. *Atmosphere*, *21*(1), 109–121. https://doi.org/10.14191/Atmos.2011.21.1.109

Shin, J. Y., Kwon, H. H., Lee, J. H., & Kim, T. W. (2020). Probabilistic long-term hydrological drought forecast using Bayesian networks and drought propagation. *Meteorological Applications*, *27*(1), e1827. https://doi.org/10.1002/met.1827

Sun, J., Wang, H., & Yuan, W. (2008). Decadal variations of the relationship between the summer North Atlantic Oscillation and middle East Asian air temperature. *Journal of Geophysical Research*, *113*(D15), D15107. https://doi.org/10.1029/2007jd009626

Sung, M. K., Kwon, W. T., Baek, H. J., Boo, K. O., Lim, G. H., & Kug, J. S. (2006). A possible impact of the North Atlantic Oscillation on the east Asian summer monsoon precipitation. *Geophysical Research Letters*, *33*(21), L21713. https://doi.org/10.1029/2006gl027253

Tsakiris, G., & Vangelis, H. (2004). Towards a drought watch system based on spatial SPI. *Water Resources Management*, *18*, 1–12. https://doi.org/10.1023/b:warm.0000015410.47014.a4

Wilhite, D. A., & Glantz, M. H. (1985). Understanding: The drought phenomenon: The role of definitions. *Water International*, *10*(3), 111–120. https://doi.org/10.1080/02508068508686328

Woodward, D. E., Hawkins, R. H., Jiang, R., Hjelmfelt, A. T., Jr., Van Mullem, J. A., & Quan, Q. D. (2003). Runoff curve number method: Examination of the initial abstraction ratio. In *World water & environmental resources congress 2003* (pp. 1–10).

Wu, W., Geller, M. A., & Dickinson, R. E. (2002). A case study for land model evaluation: Simulation of soil moisture amplitude damping and phase shift. *Journal of Geophysical Research*, *107*(D24), ACL20-1–ACL20-13. https://doi.org/10.1029/2001JD001405

Wu, Z., Wang, B., Li, J., & Jin, F. F. (2009). An empirical seasonal prediction model of the East Asian summer monsoon using ENSO and NAO. *Journal of Geophysical Research*, *114*(D18), D18120. https://doi.org/10.1029/2009jd011733

Xie, S. P., Hu, K., Hafner, J., Tokinaga, H., Du, Y., Huang, G., & Sampe, T. (2009). Indian Ocean capacitor effect on Indo–western Pacific climate during the summer following El Niño. *Journal of Climate*, *22*(3), 730–747. https://doi.org/10.1175/2008jcli2544.1

Yeo, S. R., Yeh, S. W., & Lee, W. S. (2019). Two types of heat wave in Korea associated with atmospheric circulation pattern. *Journal of Geophysical Research: Atmospheres*, *124*(14), 7498–7511. https://doi.org/10.1029/2018jd030170

Zhao, L., Wu, J., & Fang, J. (2016). Robust response of streamflow drought to different timescales of meteorological drought in Xiangjiang River Basin of China. *Advances in Meteorology*, *2016*, 1–8. https://doi.org/10.1155/2016/1634787

Zheng, X., & Eltahir, E. A. (1998). A soil moisture–rainfall feedback mechanism: 2. Numerical experiments. *Water Resources Research*, *34*(4), 777–785. https://doi.org/10.1029/97wr03497